CANCER

The long noncoding RNA *SPRIGHTLY* acts as an intranuclear organizing hub for pre-mRNA molecules

Bongyong Lee,[1] Anupama Sahoo,[1] John Marchica,[1] Erwin Holzhauser,[2] Xiaoli Chen,[2] Jian-Liang Li,[1] Tatsuya Seki,[1,3] Subramaniam Shyamala Govindarajan,[1] Fatu Badiane Markey,[4] Mona Batish,[4] Sonali J. Lokhande,[5] Shaojie Zhang,[2] Animesh Ray,[5,6] Ranjan J. Perera[1]*

Molecular mechanisms by which long noncoding RNA (lncRNA) molecules may influence cancerous condition are poorly understood. The aberrant expression of *SPRIGHTLY* lncRNA, encoded within the drosophila gene homolog *Sprouty-4* intron, is correlated with a variety of cancers, including human melanomas. We demonstrate by SHAPE-seq and dChIRP that *SPRIGHTLY* RNA secondary structure has a core pseudoknotted domain. This lncRNA interacts with the intronic regions of six pre-mRNAs: *SOX5*, *SMYD3*, *SND1*, *MEOX2*, *DCTN6*, and *RASAL2*, all of which have cancer-related functions. Hemizygous knockout of *SPRIGHTLY* by CRISPR (clustered regularly interspaced short palindromic repeats)/Cas9 in melanoma cells significantly decreases *SPRIGHTLY* lncRNA levels, simultaneously decreases the levels of its interacting pre-mRNA molecules, and decreases anchorage-independent growth rate of cells and the rate of in vivo tumor growth in mouse xenografts. These results provide the first demonstration of an lncRNA's three-dimensional coordinating role in facilitating cancer-related gene expression in human melanomas.

INTRODUCTION

Protein-coding genes constitute only 1.5 to 2% of our genome, and yet, ~75% of the human genome is transcribed; thus, most transcripts are noncoding RNAs (ncRNAs) (*1*). Small ncRNAs are now recognized participants in cancer initiation and progression (*2*, *3*). In recent years, long ncRNAs (lncRNAs) have emerged as three-dimensional spatial regulatory molecules, coordinating the expression of multiple genes at distant or unlinked genomic domains (*4*–*7*). There are approximately 58,648 lncRNA genes (*8*). The biological functions of most lncRNAs are unknown; a few of these appear to regulate various cellular processes, including chromatin organization, transcription, and RNA processing (*9*–*11*). Emerging techniques for identifying protein-associated RNA and DNA molecules by direct sequencing are playing important roles in dissecting lncRNA function. For example, the lncRNA *XIST* interacts with as many as 81 diverse proteins involved in chromatin modification, the nuclear matrix, and RNA remodeling complexes (*12*). The existence of this spatial organizing machinery was repeatedly considered in the past, but direct evidence has been lacking until recently.

The expression of the lncRNA *SPRIGHTLY* (formerly known as *SPRY4-IT1*) is up-regulated in a variety of cancers (*13*–*19*), including melanoma and prostate cancer. *SPRIGHTLY* knockdown in melanoma and prostate cancer cell lines inhibited cellular proliferation and invasiveness and increased apoptosis (*20*, *21*).

Here, we report the comprehensive mapping of *SPRIGHTLY* secondary structure by 2′-hydroxyl acylation analyzed by primer extension sequencing (SHAPE-seq) and identification of domain-specific *SPRIGHTLY*-RNA interactions using domain-specific chromatin isolation by RNA purification (dChIRP) analysis. We demonstrate that *SPRIGHTLY* interacts with the intronic regions of unprocessed mRNA precursors of several target mRNAs. Specifically, all three *SPRIGHTLY* domains interact with the intronic regions of *SMYD3*, *SND1*, *MEOX2*, *SOX5*, *RASAL2*, and *DCTN6* pre-mRNAs. These RNAs are also physically associated with their respective genomic locations and, as expected, exhibit differential expression in melanoma cells. We propose that *SPRIGHTLY* coordinates the posttranscriptional regulation of a set of genes by acting as an intranuclear organizing hub, a general molecular mechanism by which a class of lncRNAs functions.

RESULTS

We adapted the method for dChIRP (*5*, *22*) to identify *SPRIGHTLY* lncRNA-associated RNA molecules. dChIRP presents higher sensitivity and specificity compared to other methods for identifying RNA-associated macromolecules (*6*, *23*, *24*). We reasoned that identification of RNA molecules specifically associating with SPRIGHTLY lncRNA by dChIRP, which is adapted to the identification of associated RNA molecules rather than chromatins, will provide comparable resolution. To design probes complementary to selected regions of *SPRIGHTLY* RNA, we experimentally determined its most probable secondary structure (Fig. 1A) by SHAPE-seq and modeling of the resultant sequence fragments (*25*). The sugar backbone of the first approximately 120 nucleotides (nt) of *SPRIGHTLY* are moderately reactive, the next 500 nt are highly reactive, whereas the remainder of the molecule is relatively less reactive (Fig. 1B). The secondary structure model exhibits a central pseudoknotted domain and three other flexible finger-like domains with intrastrand bulges and loops. Using this structure as a guide, we were able to design a set of probes to pull down *SPRIGHTLY* lncRNA and its interacting partners, as described below.

To identify *SPRIGHTLY*-interacting RNA partners, we performed a modified dChIRP assay (fig. S1A and table S1) (*5*) by hybridizing twelve biotinylated probes (P1 to P12) (Fig. 1A) to formaldehyde–cross-linked cellular RNA, followed by streptavidin pulldown, successive elimination of the associated chromatin proteins and DNA by proteinase and deoxyribonuclease (DNase) treatments, respectively, reverse transcription of the RNA, and sequencing of the resultant molecules. The region spanned by P1 to P4 was arbitrarily labeled D1, the region spanned by P5 to P8 was labeled D2, and the region spanned by P9 to P12 was labeled D3 (fig. S1A). The pulldown efficiency of each *SPRIGHTLY* region was determined by reverse transcriptase–mediated quantitative polymerase chain reaction

[1]Sanford Burnham Prebys Medical Discovery Institute, 6400 Sanger Road, Orlando, FL 32827, USA. [2]Department of Computer Science, University of Central Florida, Orlando, FL 32816, USA. [3]Medical and Biological Laboratories, Nagoya 460-0008, Japan. [4]Department of Microbiology, Biochemistry and Molecular Genetics, Rutgers Biomedical and Health Sciences, Rutgers University, Newark, NJ 07103, USA. [5]Keck Graduate Institute, 535 Watson Drive, Claremont, CA 91711, USA. [6]Division of Biology and Biological Engineering, California Institute of Technology, Pasadena, CA 91125, USA. *Corresponding author. Email: rperera@sbpdiscovery.org

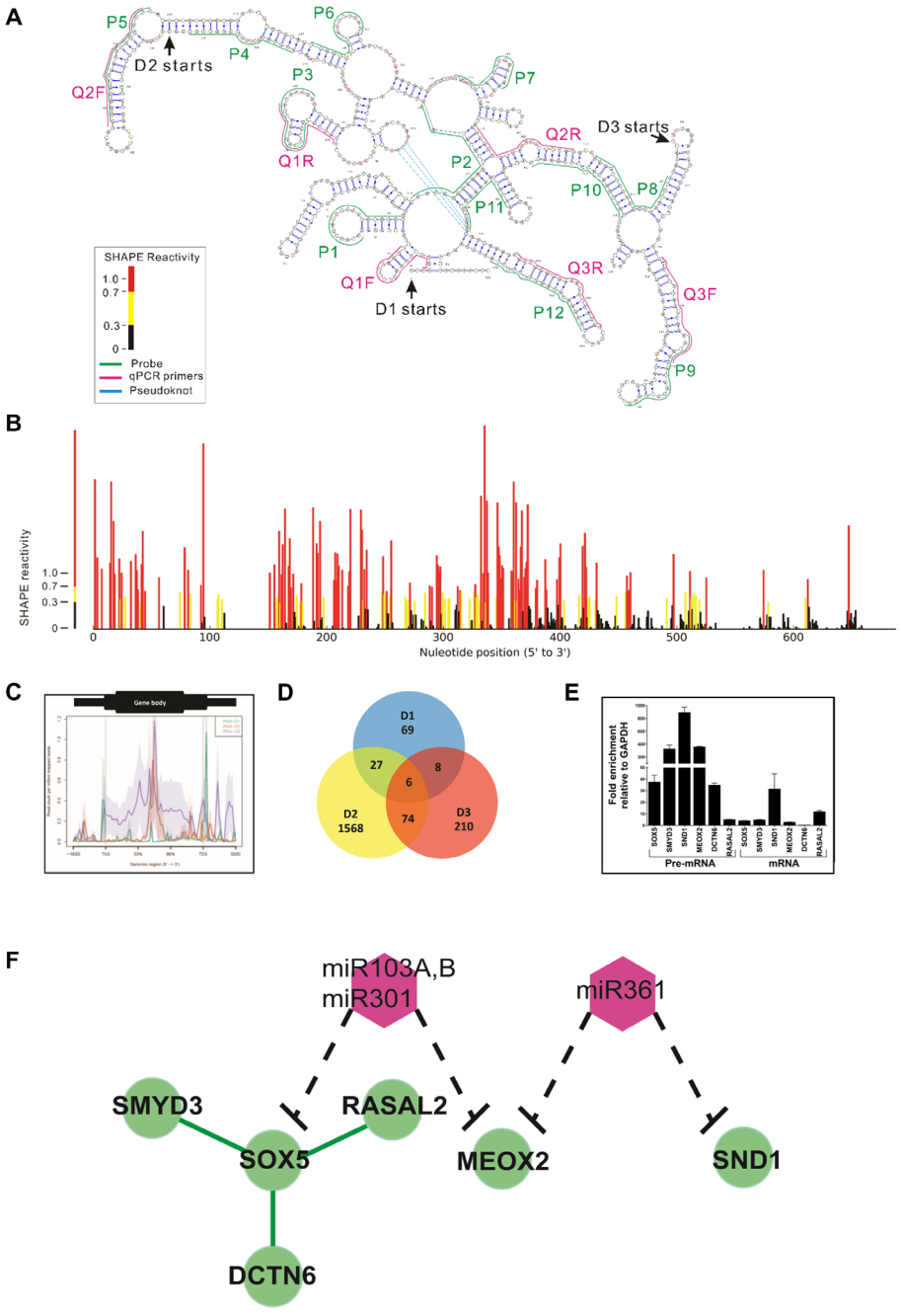

Fig. 1. *SPRIGHTLY* RNA secondary structure and its binding partners. (**A**) The secondary structure of *SPRIGHTLY* was determined by RNA structure with the constraints of SHAPE-seq reactivity data. Nucleotides are colored by their normalized reactivities ρ. The probe sequences are labeled P1 to P12. In the text, the 12 primers are termed in three sets: Set D1 is represented by probes P1 to P4, D2 is represented by probes P5 to P8, and D3 is represented by probes P9 to P12. The core pseudoknotted domain overlaps D1, D2, and D3. (**B**) Histogram of normalized SHAPE-seq reactivities as a function of nucleotide position of *SPRIGHTLY*. (**C**) The distribution of RNA sequences within gene bodies corresponding to dChIRP MACS peaks pulled down by the three sets of *SPRIGHTLY* probes, D1, D2, and D3. dChIRP MACS peaks found in the exonic region including promoter-TSS, exon, 3′UTR, and TTS were plotted. The aggregate plots of RNA dChIRP sequences peaks show the enriched regions distributed across 5000 base pairs (bp) upstream of gene bodies and 5000 bp downstream of the genes. The shades represent the SEM. Green peaks represent RNA pulled down by probes of D1, orange peaks represent RNA pulled down by probes of D2, and purple peaks represent RNA pulled down by probes of D3. (**D**) *SPRIGHTLY* binding partner RNAs determined by common MACS peaks. The MACS peaks were mapped to their corresponding genomic loci, and the number of genes was counted. If MACS peaks from individual dChIRP sequencing overlapped or mapped to same gene, then those genes were regarded as *SPRIGHTLY* binding partners. Six genes have MACS peaks common to all three regions, suggesting that those six genes are most likely to interact with *SPRIGHTLY*. (**E**) *SPRIGHTLY* dChIRP specifically enriches the intronic regions of six genes. *SPRIGHTLY* dChIRP samples were analyzed by qPCR using primers for representative MACS peak of each gene or using primers for exon-exon junctions. Each intronic region corresponding to MACS peak was enriched >5- to 800-fold over the abundant glyceraldehyde-3-phosphate dehydrogenase (*GAPDH*) mRNA. An average of three technical replicates ± SD is shown. (**F**) The integrated network of six RNA molecules that bind to *SPRIGHTLY* was constructed by querying integrated gene interaction network data. Green interaction edges represent high-confidence genetic interaction data from Lin *et al.* (*51*), and black dashed edges represent consensus miRNA target sequences (*52*).

(qPCR) using domain-specific primers (table S1). *LacZ* antisense oligonucleotides were used as negative controls, and background pulldown of nonspecific materials was negligible (fig. S1A). A total of 3483 sequence peaks (normalized against the input material) were pulled down [false discovery rate (FDR), <0.05] and were mapped to the genome (version Hg19). Of these, 155 RNA sequences were enriched by D1 probes (P1 to P4), 2896 were enriched by D2 (P5 to P8), and 432 were enriched by D3 probes (P9 to P12). One hundred eighteen RNA peaks were common between D1 and D2, 41 were common between D1 and D3, 232 were common between D2 and D3, and 36 were common to all three domains. The RNA peak identities, determined by model-based analysis of captured sequences (MACS), are listed in table S2. To confirm domain specificities of the MACS peaks, we performed qPCR with MACS peak–specific primers using the dChIRP materials. As expected, each MACS peak was enriched in a domain-specific manner (fig. S1, B and C). For example, MACS peak number 14 pulled down by D1 probes P1 to P4 was mainly enriched in D1 pulldown RNA peaks, but not in D2 or D3 pulldown RNA peaks.

We mapped the RNA MACS peaks to their respective genomic functional regions: promoter-TSS (transcription start site), exon, intron, TTS (transcription termination site), 3′UTR (3′ untranslated region), and intergenic regions (fig. S1D). The majority (52 to 68%) of RNA MACS peaks corresponded to the intronic regions of coding genes. Less frequently (21 to 30%), they were spread across multiple loci corresponding to intergenic regions—a result reminiscent of previous observations with *U1* and *MALAT1* lncRNA-interacting chromatin peaks (*7*). The enriched RNA MACS peaks were distributed across the coding and ncRNA regions of various repeat elements [short interspersed nuclear element (SINE), long interspersed nuclear element (LINE), long terminal repeat (LTR), transposable element (TE), simple repeats, and satellite sequences] (fig. S2). There were significantly fewer SINE element-encoded RNA sequences associated with the D3 region than with the other two regions of SPRIGHTLY. However, the highest mean fold enrichment of associated RNA was observed with the D3 region, followed by the D1 and D2 regions (fig. S1E). D1 shows high affinity to both TSSs (present in pre-mRNAs) and TTSs, whereas D2 and D3 mainly interact with RNA sequences embedded within gene bodies (Fig. 1C). For D2, the mean overall fold enrichment of RNA sequences corresponding to exons was statistically significantly higher than those for intronic or intergenic RNA sequences (fig. S3).

We next identified *SPRIGHTLY*-interacting RNA partners and found that D1 interacted with RNA sequences corresponding to 110 coding genes, D2 with 1675 genes, and D3 with 298 genes (Fig. 1D). RNAs belonging to six genes (*SOX5*, *SMYD3*, *SND1*, *MEOX2*, *DCTN6*, and *RASAL2*) interacted with all three regions (table S3). The pulldown sequences of these six genes' encoded RNA molecules corresponded to the intronic regions of their corresponding pre-mRNAs, and the recovered sequences were distributed across the introns of their pre-mRNAs (table S3). dChIRP was repeated, and all six *SPRIGHTLY*-interacting partner pre-mRNAs were validated by qPCR analysis (Fig. 1E) using two primer sets corresponding to the introns and the two spanning exons of these mRNAs, to distinguish between pre-mRNAs and spliced mRNAs corresponding to their respective MACS peaks.

LncRNAs are thought to coordinate the spatial organization of chromatins such that genes that map to distant regions are coordinately transcriptionally regulated (*9*). We sought to investigate a variant of this hypothesis: Pre-mRNA molecules encoded by genetically unlinked but functionally related genes are tethered by *SPRIGHTLY*. To test this hypothesis, we examined whether the mRNAs enriched in the dChIRP material were functionally related. Gene sets with common function ought to be enriched in common gene ontology (GO) annotations, and these gene groups should be enriched for known genetic or physical interactions of their respective protein products because these interactions embody functional relatedness. Consistent with this hypothesis, 115 protein-coding genes corresponding to mRNAs pulled down by the D1-D2, D1-D3, and D2-D3 region pairs (Fig. 1D), and all three regions combined, were enriched for protein phosphorylation and neuron-related GO functional terms (table S4). There was significant (FDR-corrected, $P = 6.64 \times 10^{-3}$) functional enrichment for cell motility function, represented by the following genes: *FYN*, *EPHA3*, *PFN2*, *STK10*, *HSP90AA1*, *MEF2C*, *RBFOX2*, *PDE4D*, *RERE*, *CDC42BPA*, *CDH2*, *GPC6*, and *PDE4B*. Of these, *RBFOX2* and *RERE* are important for glial cell–guided neuron migration in the hindbrain (*26*, *27*). We examined the four GO-enriched D2-D3 gene subsets (table S5) by querying databases of physical (protein-protein) and genetic interaction networks. The known genetic or physical interactions within these gene groups, separately queried according to their GO annotation categories, are shown in fig. S4 (A to D). Functional analysis of the D2 and D3 region gene subnetworks (with at least seven genes in the respective sets) revealed significant enrichment for the microtubule-organizing center, protein phosphorylation, cell migration, and regulation of neuron projection development functions (table S5). When the genes corresponding to the set of 74 mRNAs pulled down by D2 and D3 regions were queried together, they constituted a 60-member interaction network densely interconnected by numerous known genetic interaction edges (fig. S4E), suggesting a high degree of functional overlap. In addition to the genes enriched by D2-D3 pulldown, we examined the genes corresponding to the set of six mRNAs pulled down by all three domains. This six-gene subset constituted a connected network of genes related by known genetic interactions and as putative co-regulated targets of two microRNAs (miRNAs) that were previously identified as important for cancers of the lungs, breast, liver, and pancreas (Fig. 1F).

To investigate the dependence of expression levels of the six binding partners on *SPRIGHTLY*, we knocked out *SPRIGHTLY* by using CRISPR (clustered regularly interspaced short palindromic repeats)/Cas9. Two guide RNAs targeting the upstream and downstream regions of *SPRIGHTLY* (fig. S5A) were introduced to cells stably expressing Cas9p. Single-cell clones were isolated, and PCR analysis of genomic DNA demonstrated that one allele had the appropriate deletion to produce hemizygous *SPRIGHTLY* knockout in the SC2-17 cells (fig. S5B). *SPRIGHTLY* expression levels in SC2-17 cells decreased by approximately 80% compared to those of the parental cells (fig. S5C).

To confirm that *SPRIGHTLY* lncRNA colocalizes with its target pre-mRNA molecules, we applied dual RNA-FISH (fluorescence in situ hybridization) assays on A375 and SC2-17 cells (Fig. 2, A to F). We designed single-molecule FISH (smFISH) probes specific for *SPRIGHTLY* and found that *SPRIGHTLY* lncRNA is primarily localized in the cell nucleus (Fig. 2B). We did not detect RNA-FISH signals for *SPRIGHTLY* in SC2-17 cells, suggesting that hemizygous deletion of *SPRIGHTLY* causes a sharp decrease in *SPRIGHTLY* RNA expression (Fig. 2, B and F). Statistically significant colocalization of *SPRIGHTLY* lncRNA and its partner pre-mRNAs encoded by *SMYD3* and *SND1* (Fig. 2, D, E, and G) confirms the genome-wide dChIRP data on these two RNAs (Fig. 1E) and also reinforces the idea that physical association between *SPRIGHTLY* and these two pre-mRNA molecules is functionally relevant. To investigate the effects of this physical association on mRNA expression levels, we next measured the expression levels of the six *SPRIGHTLY* binding partner RNAs by qPCR. As shown in Fig. 2H, both mRNA and pre-mRNA levels of *SMYD3*, *SOX5*, and *RASAL2* were

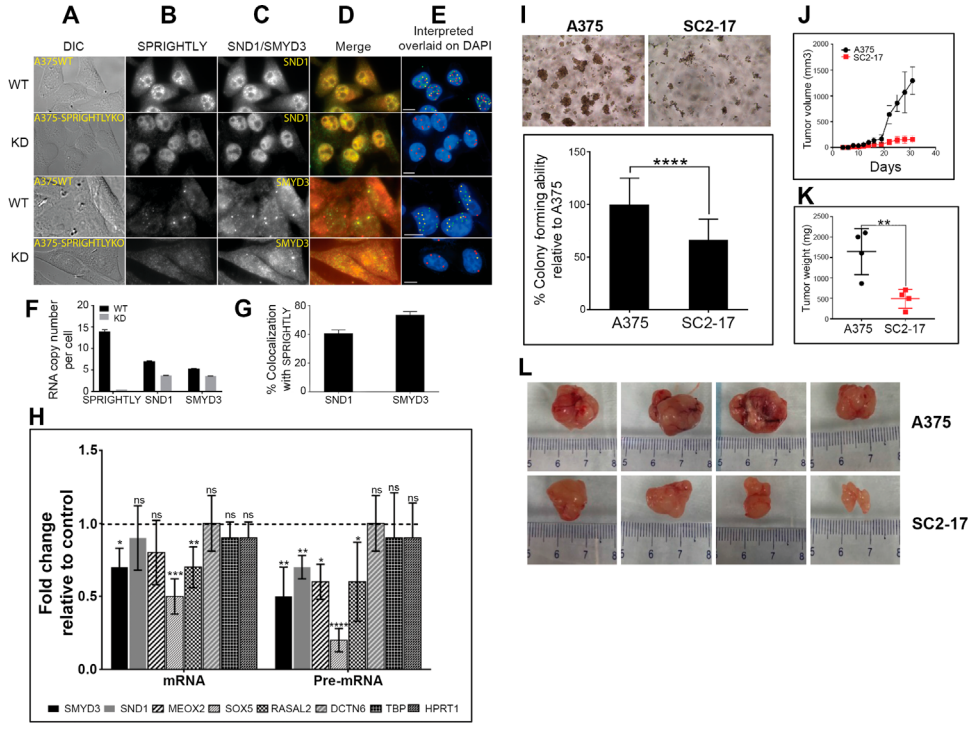

Fig. 2. *SPRIGHTLY* hemizygous knockout suppresses anchorage-independent growth in vitro and the tumor growth in vivo. (**A** to **G**) Colocalization between *SPRIGHTLY* and intronic regions of *SMYD3* and *SND1*: (A) the differential interference contrast (DIC) image of parental and knockout cells, (B) raw image showing *SPRIGHTLY* RNA probed using smFISH probes labeled with Texas Red, (C) raw images showing *SND1* RNA (top two panels), and *SMYD3* RNA (bottom two panels) probed using probes labeled with tetramethylrhodamine (TMR). (D) Merge of RNA spots for *SPRIGHTLY* are pseudocolored as green, and *SND1* and *SMYD3* are pseudocolored as red. (E) The spots were identified using custom-written algorithms in MATLAB. WT, wild type; KD, knockdown. The identified spots are overlaid over 4′,6-diamidino-2-phenylindole (DAPI) staining as red (*SND1*/*SMYD3*), green (*SPRIGHTLY*), and yellow (colocalized) circles. (F) Quantification of about 50 cells to determine the copy number. (G) Extent of colocalization of *SND1* and *SMYD3* with *SPRIGHTLY* lncRNA. The error bars represent 95% confidence interval. Scale bars, 5 μm. (**H**) *SPRIGHTLY* hemizygous knockout decreased the expression levels of both mRNA and pre-mRNA of RNA binding partners. The expression levels were measured in both A375 and SC2-17 cells by qPCR. The expression levels of both mRNA and pre-mRNA of *TBP* or *HPRT1* were not affected by *SPRIGHTLY* in SC2-17 cells. Delta threshold cycle (ΔC_t) was calculated by subtracting the average C_t value of *ACTB*, *TBP*, and *HPRT1* from the C_t value of target gene. The data were obtained from three independent experiments and are expressed as means ± SD. ns, not significant. *$P \leq 0.05$, **$P \leq 0.01$, ***$P \leq 0.001$, ****$P \leq 0.0001$, Student's *t* test. (**I**) A375 and SC2-17 cells were seeded and cultured for 7 days. Shown is a representative image of impaired colony-forming ability in SC2-17 cells compared to control cells (A375). The MTT assay was used to determine cell number. Results are expressed as means ± SD from six independent experiments. ****$P \leq 0.0001$, Student's *t* test. (**J** to **L**) Five-week-old female SCID mice were subcutaneously injected with either A375 or SC2-17 cells ($n = 4$ mice per group). (J) Graph depicts tumor volume (volume = $(\text{width})^2 \times \text{length}/2$) observed for the A375 and SC2-17 groups at different time points until the tumors were excised. (K) Approximately 1 month after implantation, mice were euthanized, and tumors were excised and weighed. Graph depicts tumor weight (in milligrams) of A375 and SC2-17 tumor xenografts. (L) Images of the excised tumors on a scale bar are shown. Student's *t* test was performed to detect between-group differences. The data in (J) and (K) are representative of at least three independent experiments with consistent results. **$P \leq 0.01$, Student's *t* test.

significantly decreased in SC2-17 cells relative to those in A375 cells. Whereas pre-mRNA levels were decreased, no changes were observed in the mature mRNA levels of *SND1* and *MEOX2* genes.

To investigate the role of *SPRIGHTLY* in cancer development, we monitored anchorage-independent growth of hemizygous *SPRIGHTLY* knockout SC2-17 cells and compared them with those of their parental A375 cells. Cells were cultured in a semisolid culture medium, and their colony-forming ability was measured (Fig. 2I) by the MTT [3-(4, 5-dimethylthiazolyl-2)-2,5-diphenyltetrazolium bromide] assay. There was a significant reduction in colony formation ability of *SPRIGHTLY* knockout cells compared to that of parental cells, and the reduction was reversed by complementation with the *SPRIGHTLY* gene under a constitutive promoter (fig. S6A). The ectopic expression of *SPRIGHTLY* in SC2-17 cells recovered the expression levels of its RNA binding partners (fig. S6B). We next determined the profile of *SPRIGHTLY*-dependent gene expression by RNA sequencing (RNA-seq) conducted on parental A375 and hemizygous *SPRIGHTLY* knockout SC2-17 cells. In the knockout line, 117 genes were significantly down-regulated ($-1.3 \geq \log_2(\text{ratio}) \geq -9.4$; $4.2 \times 10^{-16} \leq$ FDR-corrected $P \leq 0.05$). This down-regulated gene set overlapped with genes (*28*) in the cancer modules #112 (FDR-corrected, $P = 9.9 \times 10^{-8}$) and #55 (FDR-corrected, $P = 1.11 \times 10^{-3}$), respectively, with genes in the cell signaling module #176 (FDR-corrected, $P = 5.98 \times 10^{-8}$), with genes in the neural development gene modules #2 (FDR-corrected, $P = 2.9 \times 10^{-5}$) and #12 (FDR-corrected, $P = 2.24 \times 10^{-5}$), respectively, and with the genes in immune and inflammatory response module #84 (FDR-corrected, $P = 4.65 \times 10^{-5}$). Finally, we investigated *SPRIGHTLY*'s in vivo biological role in xenografts on severe combined immunodeficient (SCID) mice. Whereas control A375 cells were readily able to form subcutaneous tumors in SCID mice, SC2-17 cells exhibited significantly reduced tumorigenicity. The tumor volume differences became apparent by day 20 (Fig. 2J) and were confirmed by measuring the tumor weight and size after sacrificing the mice at day 31 (Fig. 2, K and L).

DISCUSSION

By adapting ncRNA-associated chromatin precipitation and identification technique to identifying *SPRIGHTLY*-interacting RNA molecules, we discovered that this lncRNA interacted with more than 2000 different high-confidence RNA molecules. To do this, we analyzed the topological shape of *SPRIGHTLY*, and guided by its structure, we designed three sets of probes that interrogated three overlapping structural domains, D1, D2, and D3, including a predicted pseudoknotted core structure. Not all the ~2000 high-confidence binding partners may be authentic; however, those RNAs that bind to two domains each, and especially the six RNA molecules (*SOX5*, *SMYD3*, *SND1*, *MEOX2*, *DCTN6*, and *RASAL2*) that are bound to all three domains, represent high-confidence interaction partners of *SPRIGHTLY*. On the basis of the distribution and topological overlaps of the three sets of probes complementary to the three structural domains of *SPRIGHTLY*, we infer that these six highest-confidence interacting RNA molecules are likely to interact with structural features that are common to all three regions—namely, the pseudoknotted central core minimally overlapping P2 (of D1), P7 (of D2), and P11 (of D3). Future in vitro cross-linking experiments with purified *SPRIGHTLY* and the pre-mRNAs transcribed off these genes will be necessary to test this prediction.

Our observations that *SPRIGHTLY* was more frequently associated with RNA sequences corresponding to the intronic regions of protein-coding RNAs and less frequently with RNAs expressed from intergenic regions are consistent with previous observations with *U1* and *MALAT1* lncRNA-interacting chromatin peaks (*7*). The chromatin regions corresponding to introns of protein-coding genes are more frequently associated with these two lncRNAs relative to intergenic regions. If this correspondence between RNA- and chromatin-interacting partners holds also for *SPRIGHTLY* chromatin binding (not investigated here), then these results would imply that lncRNAs are intimately associated with selected chromatin regions in large supramolecular assemblies that include both chromatin and nascent pre-mRNAs transcribed off those chromatin regions. RNA sequences corresponding to promoter-TSS regions, exons, TTS, and 3′UTRs were relatively infrequently associated with the three structural domains of *SPRIGHTLY* compared to the intronic and intergenic ncRNA regions. Although the numbers of RNA MACS peak enrichment were different for all three domains, the normalized intronic enrichment percentages were similar.

The six genes that encode the highest-confidence pre-mRNA binding partners of *SPRIGHTLY* were previously identified to play important roles in cancer. The transcription factor SOX5 negatively regulates microphthalmia-associated transcription factor, whose level is low in invasive melanoma cells, by competing with SOX10 for promoter binding sites in normal melanocytes (*29*). *SMYD3* encodes histone H3-K4 di-/trimethyltransferase and H4-K5-methyltransferase activities, causes transcriptional activation, and regulates the expression of critical cancer-associated proteins, such as the androgen receptor, c-Met, telomerase reverse transcriptase, and matrix metalloproteinase 9 (*30*, *31*). SMYD3 overexpression is associated with brain tumors and colorectal, hepatocellular, breast, and prostate cancers (*32*–*35*). *SND1* encodes a Tudor domain nuclease, whose expression is associated with metastatic melanoma, and was initially identified as a transcriptional coactivator of PIM1-mediated control of C-MYB expression and later as a component of the RNA-induced silencing complex (*36*). *SND1* modulates transcriptional activation, RNA splicing, RNA editing, RNA stability, and RNAi function; promotes invasion, proliferation, migration, and angiogenesis in liver cancer; and promotes invasion and metastasis in breast cancer (*37*). *SND1* knockdown reduces prostate cancer cell line proliferation rate (*38*), and its high expression is associated with colorectal cancer and malignant glioma (*39*, *40*). The finding that these six pre-mRNA molecules are associated with *SPRIGHTLY* at the highest confidence level suggests that *SPRIGHTLY* predominantly interacts with these six pre-mRNA molecules, presumably through *SPRIGHTLY*'s pseudoknotted central core, and that the interaction targets the introns of unspliced RNA molecules. Results of statistical analysis of functional enrichment of gene sets associated with *SPRIGHTLY* are also consistent with the hypothesis that *SPRIGHTLY* lncRNA binds to many more functionally related pre-mRNA molecules than just the six highest-confidence pre-mRNAs, which, at the very least, are encoded by genes important for cell motility, migration, neuronal migration, and cancers in general.

We have tested the hypothesis that the transcript levels from selected target genes might be controlled by *SPRIGHTLY*, by analyzing the coordinate expression of pre-mRNA and mature mRNA from the six genes in cells harboring a hemizygous knockout of *SPRIGHTLY*. The knockout event is associated with ~80% reduction in *SPRIGHTLY* RNA levels. The results indicate that *SMYD3*, *SOX5*, and *RASAL2* mRNA levels are directly regulated through a common mechanism involving *SPRIGHTLY*, which is also supported by the existence of genetic interaction among these four genes (Fig. 1F). The influence of *SPRIGHTLY* on the other two mRNAs might be indirect and more complex, because their pre-mRNA levels but not their mature mRNA levels were perturbed in the hemizygous knockout cells.

RNA-seq analysis in cell lines with or without the hemizygous knockout demonstrated that RNA levels of gene sets with provocative functions in melanoma and brain metastasis are significantly reduced when *SPRIGHTLY* expression is reduced. This is exactly the result anticipated if *SPRIGHTLY* lncRNA increases the expression of tumor- and metastasis-related genes, including those potentially important for metastasis into neural tissues. As expected, mouse xenograft studies with unmodified and *SPRIGHTLY* knockout melanoma cell lines confirmed that tumor growth rates were directly correlated with *SPRIGHTLY* expression levels.

In conclusion, we have provided evidence demonstrating that *SPRIGHTLY* lncRNA acts as a posttranscriptional nuclear hub by binding to the intronic regions of a set of pre-mRNA molecules that are enriched for cancer-related functions, especially those related to cell motility as well as cell migration into the brain, and thereby regulates the latter's biological functions. This has significant implications, because more than 60% of deaths from invasive melanoma are due to metastasis to the brain (*41*).

MATERIALS AND METHODS

Tissue culture

A375 cells (American Type Culture Collection, CRL-1619) were grown in Complete Tu Medium containing a 4:1 mixture of MCDB-153 medium with sodium bicarbonate (1.5 g/liter) and Leibovitz's L-15 medium with 2 mM L-glutamine, 2% fetal bovine serum, and 1.68 mM $CaCl_2$ (*42*). The cells were grown in a humidified incubator at 37°C, 5% CO_2.

dChIRP oligonucleotide design

Biotinylated 20-mer antisense oligonucleotides were designed using the Stellaris smFISH probe designer (http://biosearch.com/) (*6*). Designed probes were compared with the human genome using the BLAT tool, and probes returning only target were selected (table S1). For *LacZ* probes, six biotinylated 20-mer antisense oligonucleotides were prepared (*5*).

Modified dChIRP

dChIRP was performed as previously described (*5*). Cells were cross-linked with 0.3% formaldehyde for 10 min, quenched with 0.125 M glycine for 5 min, and washed with phosphate-buffered saline. Sheared chromatin was prepared by sonication using a Bioruptor 300 (Diagenode) to produce DNA between 100 and 500 bp. Chromatin was diluted three times with hybridization buffer, and probes were added (15 pmol per chromatin from 1 million cells). The mixture was incubated overnight at 37°C with rotation. Streptavidin magnetic C1 beads (Thermo Fisher Scientific Inc.) were added and mixed for another 2 hours at 37°C. After extensive washing, the beads were resuspended in a buffer containing proteinase K (Sigma-Aldrich) and incubated at 50°C for 45 min, followed by overnight incubation at 65°C for reverse cross-linking. RNAs were extracted by TRIzol/chloroform and precipitated with ethanol. The purified RNAs were treated with DNA-free reagent (Life Technologies) to eliminate DNA according to the manufacturer's protocol. DNase was inactivated by heating at 65°C for 15 min, and RNAs were quantified using a Qubit 2.0 Fluorometer (Thermo Fisher Scientific Inc.).

Sequencing and data analysis

dChIRPed RNAs were subjected to double-stranded complementary DNA synthesis using an Ovation RNA-Seq System V2 (NuGEN Technologies Inc.). High-throughput sequencing libraries were constructed using the TruSeq ChIP Sample Preparation Kit (Illumina) and sequenced on a HiSeq 2500 (Illumina) with 50-bp read lengths. Sequencing data were analyzed as previously described (*6*). dChIRP peaks were defined by MACS (*43*) as previously described (*5*). The peaks were identified by MACS2 program software, and the q value (≤0.05) was assigned as the cutoff by Benjamini-Hochberg correction.

2′-hydroxyl acylation analyzed by primer extension sequencing (SHAPE-Seq)

SPRIGHTLY RNA was prepared by in vitro transcription using the MEGAscript kit (Life Technologies) with PCR product DNA as template. RNA was purified using the Direct-zol RNA MiniPrep kit (Zymo Research). Purified RNA was heated at 95°C for 2 min, snap-cooled on ice, and refolded in a buffer containing 100 mM Hepes-KOH (pH 8.0), 100 mM NaCl, and 10 mM $MgCl_2$ for 20 min at 37°C. The refolded RNAs were treated with 6.5 mM *N*-methylisatoic anhydride (Life Technologies) at 37°C for 50 min. RNAs were recovered using RNA Clean & Concentrator-25 (Zymo Research). For sequencing, the modified RNAs were subjected to library construction, as previously described (*25*), with slight modification. Universal miRNA Cloning Linker (New England Biolabs) was used as an RNA linker, and all ethanol precipitation steps were replaced with column purification using RNA Clean & Concentrator-25 (Zymo Research). Libraries were used for nine-cycle PCR amplification with primers containing Illumina sequencing and index multiplexing and then sequenced on the Illumina HiSeq platform. Adapters and primers were listed in table S1.

SHAPE-seq data analysis

Channel reads [1,041,097 (+) and 601,817 (−)] were collected from SHAPE-seq experiments. Reverse transcriptase primers were trimmed from the reads using Cutadapt version 1.10 (*44*). Handle sequences were kept for separating (+) and (−) channel reads. Both (+) and (−) channel reads were combined into one file and then mapped to *SPRIGHTLY* by Bowtie version 1.0.0 (*45*). Spats version 1.0.0 (*46*) was performed to calculate the reactivity value for each nucleotide in *SPRIGHTLY* from the mapping result. The reactivity values θ were normalized to SHAPE-seq reactivities ρ by multiplying the length of the transcript. RNAstructure version 5.8.1 was performed to predict the secondary structure with the SHAPE-seq reactivity data. The parameters m and b were set to 1.1 and −0.3, respectively, following the guide of the SHAPE-seq 2.0 protocol (*25*). VARNA version 3.93 (*47*) was used to visualize the predicted secondary structure.

Single-molecule fluorescence in situ hybridization

A set of probes, each 20 nt long, was designed specifically to the intron 10 and 15 of SND1 (32 probes) and intron 5 of SMYD3 (48 probes). The region of probe binding was selected to overlap the MACS peak regions identified in the ChIRP analysis while avoiding any repetitive sequences. Another set of 25 probes was designed to bind *SPRIGHTLY* lncRNA. The probes were ordered from LGC Biosearch LLC with a 3′-amino modification and were coupled with either tetramethylrhodamine for the intronic probes or Texas Red for the *SPRIGHTLY* probes. The A375 cells (both wild type and the cell line with *SPRIGHTLY* knockout) were cultured on glass coverslips, fixed, permeabilized, and hybridized with lncRNA probe and one of the intron probe sets. The next day, the unbound probes were washed off, and the coverslips were mounted and imaged using a Nikon Ti-E inverted wide-field fluorescence microscope with a 100× objective and a cooled charge-coupled device pixis camera.

Image acquisition and analysis

The images were acquired using MetaMorph imaging software. We acquired approximately 30 optical slices at 0.2-μm intervals, thereby covering the entire volume of the cells. The images were analyzed to determine the numbers and colocalization between lncRNA and introns using custom-written algorithms in MATLAB (MathWorks Inc.), as described before (*48*). Briefly, the program analyzed the whole z stacks and removed nonuniform background to enhance particulate signal. The RNA spots in each channel were then identified in a semiautomated way by picking an intensity threshold. The signal below the threshold was discarded as background, and only the signal above background was considered as an RNA particle. Then, a custom-written program was used to determine the colocalization between spots in different channels, as described before (*49*). All the colocalization data were validated by using appropriate controls, as described in literature (*50*). The MATLAB program scripts are available upon request.

Soft agar colony formation assays

Anchorage-independent growth assays were performed by seeding 10,000 cells suspended in 0.3% base agar in 96-well plates coated with 0.6% base agar using a CytoSelect 96-well cell transformation assay kit (Cell Biolabs Inc.). Colonies were counted 7 days after seeding and analyzed using MTT solution provided with the kit according to the manufacturer's protocol. The data from six independent experiments were expressed as means ± SD.

GO and network analysis

GO analysis was peformed using g:Profiler. Subsets of genes that were enriched in GO function were queried against the physical protein interaction databases CORUM and BioGRID (Biological General Repository for Interaction Datasets) and a genetic interaction database to generate gene subnetworks using the GeneMANIA application from within Cytoscape.

Mouse xenograft study

Five-week-old SCID mice were purchased from Charles River Laboratories. Three to 5 days of acclimatization after arrival, the inoculation

area was shaved to remove body hair and sterilized with ethanol. A375 or SC2-17 cells (5.0×10^6 cells per site; $n = 4$ mice per group) were subcutaneously injected into the lower left flank of each mouse with a 27-gauge needle. Tumor size was monitored daily with digital calipers and documented once tumor growth became visible (after day 4). Tumor volume (in cubic millimeters) was calculated by the following formula: volume = $(\text{width})^2 \times \text{length}/2$. Mice were euthanized on day 31 after injection, and weight and pictures of excised tumors were taken.

SUPPLEMENTARY MATERIALS

Supplementary material for this article is available at http://advances.sciencemag.org/cgi/content/full/3/5/e1602505/DC1

fig. S1. The pulldown efficiency of *SPRIGHTLY* and validation of copurification of RNA binding partners by qPCR.
fig. S2. Many MACS peaks are composed of repetitive sequences.
fig. S3. The fold enrichment of dChIRP MACS peaks.
fig. S4. Gene interaction networks of *SPRIGHTLY*-interacting RNA molecules.
fig. S5. *SPRIGHTLY* knockout using a CRISPR system.
fig. S6. *SPRIGHTLY* overexpression recovered the loss of anchorage-independent growth of SC2-17 cells.
table S1. Probe and qPCR primer sequences.
table S2. List of common MACS peaks.
table S3. A list of six genes and corresponding MACS peaks.
table S4. g:Profiler of all 115 genes.
table S5. GO term analysis of genes pulled down by D2 and D3 regions.
table S6. SC2-17 RNA-seq results for six targets.

REFERENCES AND NOTES

1. S. Djebali, C. A. Davis, A. Merkel, A. Dobin, T. Lassmann, A. Mortazavi, A. Tanzer, J. Lagarde, W. Lin, F. Schlesinger, C. Xue, G. K. Marinov, J. Khatun, B. A. Williams, C. Zaleski, J. Rozowsky, M. Roder, F. Kokocinski, R. F. Abdelhamid, T. Alioto, I. Antoshechkin, M. T. Baer, N. S. Bar, P. Batut, K. Bell, I. Bell, S. Chakrabortty, X. Chen, J. Chrast, J. Curado, T. Derrien, J. Drenkow, E. Dumais, J. Dumais, R. Duttagupta, E. Falconnet, M. Fastuca, K. Fejes-Toth, P. Ferreira, S. Foissac, M. J. Fullwood, H. Gao, D. Gonzalez, A. Gordon, H. Gunawardena, C. Howald, S. Jha, R. Johnson, P. Kapranov, B. King, C. Kingswood, O. J. Luo, E. Park, K. Persaud, J. B. Preall, P. Ribeca, B. Risk, D. Robyr, M. Sammeth, L. Schaffer, L.-H. See, A. Shahab, J. Skancke, A. M. Suzuki, H. Takahashi, H. Tilgner, D. Trout, N. Walters, H. Wang, J. Wrobel, Y. Yu, X. Ruan, Y. Hayashizaki, J. Harrow, M. Gerstein, T. Hubbard, A. Reymond, S. E. Antonarakis, G. Hannon, M. C. Giddings, Y. Ruan, B. Wold, P. Carninci, R. Guigo, T. R. Gingeras, Landscape of transcription in human cells. *Nature* **489**, 101–108 (2012).
2. C. M. Croce, Causes and consequences of microRNA dysregulation in cancer. *Nat. Rev. Genet.* **10**, 704–714 (2009).
3. A. Lujambio, S. W. Lowe, The microcosmos of cancer. *Nature* **482**, 347–355 (2012).
4. M. Huarte, The emerging role of lncRNAs in cancer. *Nat. Med.* **21**, 1253–1261 (2015).
5. J. J. Quinn, I. A. Ilik, K. Qu, P. Georgiev, C. Chu, A. Akhtar, H. Y. Chang, Revealing long noncoding RNA architecture and functions using domain-specific chromatin isolation by RNA purification. *Nat. Biotechnol.* **32**, 933–940 (2014).
6. C. Chu, K. Qu, F. L. Zhong, S. E. Artandi, H. Y. Chang, Genomic maps of long noncoding RNA occupancy reveal principles of RNA-chromatin interactions. *Mol. Cell* **44**, 667–678 (2011).
7. J. M. Engreitz, K. Sirokman, P. McDonel, A. A. Shishkin, C. Surka, P. Russell, S. R. Grossman, A. Y. Chow, M. Guttman, E. S. Lander, RNA-RNA interactions enable specific targeting of noncoding RNAs to nascent Pre-mRNAs and chromatin sites. *Cell* **159**, 188–199 (2014).
8. M. K. Iyer, Y. S. Niknafs, R. Malik, U. Singhal, A. Sahu, Y. Hosono, T. R. Barrette, J. R. Prensner, J. R. Evans, S. Zhao, A. Poliakov, X. Cao, S. M. Dhanasekaran, Y.-M. Wu, D. R. Robinson, D. G. Beer, F. Y. Feng, H. K. Iyer, A. M. Chinnaiyan, The landscape of long noncoding RNAs in the human transcriptome. *Nat. Genet.* **47**, 199–208 (2015).
9. J. L. Rinn, H. Y. Chang, Genome regulation by long noncoding RNAs. *Annu. Rev. Biochem.* **81**, 145–166 (2012).
10. S. Geisler, J. Coller, RNA in unexpected places: Long non-coding RNA functions in diverse cellular contexts. *Nat. Rev. Mol. Cell Biol.* **14**, 699–712 (2013).
11. K. W. Vance, C. P. Ponting, Transcriptional regulatory functions of nuclear long noncoding RNAs. *Trends Genet.* **30**, 348–355 (2014).
12. C. Chu, Q. C. Zhang, S. T. da Rocha, R. A. Flynn, M. Bharadwaj, J. M. Calabrese, T. Magnuson, E. Heard, H. Y. Chang, Systematic discovery of Xist RNA binding proteins. *Cell* **161**, 404–416 (2015).
13. X. L. Zhao, Z. H. Zhao, W. C. Xu, J. Q. Hou, X. Y. Du, Increased expression of SPRY4-IT1 predicts poor prognosis and promotes tumor growth and metastasis in bladder cancer. *Int. J. Clin. Exp. Pathol.* **8**, 1954–1960 (2015).
14. Y. Shi, J. Li, Y. Liu, J. Ding, Y. Fan, Y. Tian, L. Wang, Y. Lian, K. Wang, Y. Shu, The long noncoding RNA SPRY4-IT1 increases the proliferation of human breast cancer cells by upregulating ZNF703 expression. *Mol. Cancer* **14**, 51 (2015).
15. L. Zhang, J. Huang, N. Yang, J. Greshock, M. S. Megraw, A. Giannakakis, S. Liang, T. L. Naylor, A. Barchetti, M. R. Ward, G. Yao, A. Medina, A. O'Brien-Jenkins, D. Katsaros, A. Hatzigeorgiou, P. A. Gimotty, B. L. Weber, G. Coukos, microRNAs exhibit high frequency genomic alterations in human cancer. *Proc. Natl. Acad. Sci. U.S.A.* **103**, 9136–9141 (2006).
16. H. W. Xie, Q. Q. Wu, B. Zhu, F. J. Chen, L. Ji, S. Q. Li, C. M. Wang, Y. S. Tong, L. Tuo, M. Wu, Z. H. Liu, J. Lv, W. H. Shi, X. F. Cao, Long noncoding RNA SPRY4-IT1 is upregulated in esophageal squamous cell carcinoma and associated with poor prognosis. *Tumour Biol.* **35**, 7743–7754 (2014).
17. W. Peng, G. Wu, H. Fan, J. Wu, J. Feng, Long noncoding RNA SPRY4-IT1 predicts poor patient prognosis and promotes tumorigenesis in gastric cancer. *Tumour Biol.* **36**, 6751–6758 (2015).
18. J. Mazar, W. Zhao, A. M. Khalil, B. Lee, J. Shelley, S. S. Govindarajan, F. Yamamoto, M. Ratnam, M. N. Aftab, S. Collins, B. N. Finck, X. Han, J. S. Mattick, M. E. Dinger, R. J. Perera, The functional characterization of long noncoding RNA SPRY4-IT1 in human melanoma cells. *Oncotarget* **5**, 8959–8969 (2014).
19. J. E. Wilusz, S. M. Freier, D. L. Spector, 3' End processing of a long nuclear-retained noncoding RNA yields a tRNA-like cytoplasmic RNA. *Cell* **135**, 919–932 (2008).
20. D. Khaitan, M. E. Dinger, J. Mazar, J. Crawford, M. A. Smith, J. S. Mattick, R. J. Perera, The melanoma-upregulated long noncoding RNA *SPRY4-IT1* modulates apoptosis and invasion. *Cancer Res.* **71**, 3852–3862 (2011).
21. B. Lee, J. Mazar, M. N. Aftab, F. Qi, J. Shelley, J.-L. Li, S. Govindarajan, F. Valerio, I. Rivera, T. Thurn, T. A. Tran, D. Kameh, V. Patel, R. J. Perera, Long noncoding RNAs as putative biomarkers for prostate cancer detection. *J. Mol. Diagn.* **16**, 615–626 (2014).
22. J. J. Quinn, H. Y. Chang, In situ dissection of RNA functional subunits by domain-specific chromatin isolation by RNA purification (dChIRP). *Methods Mol. Biol.* **1262**, 199–213 (2015).
23. M. D. Simon, C. I. Wang, P. V. Kharchenko, J. A. West, B. A. Chapman, A. A. Alekseyenko, M. L. Borowsky, M. I. Kuroda, R. E. Kingston, The genomic binding sites of a noncoding RNA. *Proc. Natl. Acad. Sci. U.S.A.* **108**, 20497–20502 (2011).
24. J. M. Engreitz, A. Pandya-Jones, P. McDonel, A. Shishkin, K. Sirokman, C. Surka, S. Kadri, J. Xing, A. Goren, E. S. Lander, K. Plath, M. Guttman, The Xist lncRNA exploits three-dimensional genome architecture to spread across the X chromosome. *Science* **341**, 1237973 (2013).
25. D. Loughrey, K. E. Watters, A. H. Settle, J. B. Lucks, SHAPE-Seq 2.0: Systematic optimization and extension of high-throughput chemical probing of RNA secondary structure with next generation sequencing. *Nucleic Acids Res.* **42**, e165 (2014).
26. C. Braeutigam, L. Rago, A. Rolke, L. Waldmeier, G. Christofori, J. Winter, The RNA-binding protein Rbfox2: An essential regulator of EMT-driven alternative splicing and a mediator of cellular invasion. *Oncogene* **33**, 1082–1092 (2014).
27. S. Fransson, T. Martinsson, K. Ejeskär, Neuroblastoma tumors with favorable and unfavorable outcomes: Significant differences in mRNA expression of genes mapped at 1p36.2. *Genes Chromosomes Cancer* **46**, 45–52 (2007).
28. A. Subramanian, P. Tamayo, V. K. Mootha, S. Mukherjee, B. L. Ebert, M. A. Gillette, A. Paulovich, S. L. Pomeroy, T. R. Golub, E. S. Lander, J. P. Mesirov, Gene set enrichment analysis: A knowledge-based approach for interpreting genome-wide expression profiles. *Proc. Natl. Acad. Sci. U.S.A.* **102**, 15545–15550 (2005).
29. C. C. Stolt, P. Lommes, S. Hillgartner, M. Wegner, The transcription factor Sox5 modulates Sox10 function during melanocyte development. *Nucleic Acids Res.* **36**, 5427–5440 (2008).
30. G. S. Van Aller, N. Reynoird, O. Barbash, M. Huddleston, S. Liu, A.-F. Zmoos, P. McDevitt, R. Sinnamon, B. Le, G. Mas, R. Annan, J. Sage, B. A. Garcia, P. J. Tummino, O. Gozani, R. G. Kruger, Smyd3 regulates cancer cell phenotypes and catalyzes histone H4 lysine 5 methylation. *Epigenetics* **7**, 340–343 (2012).
31. R. Hamamoto, Y. Furukawa, M. Morita, Y. Iimura, F. P. Silva, M. Li, R. Yagyu, Y. Nakamura, *SMYD3* encodes a histone methyltransferase involved in the proliferation of cancer cells. *Nat. Cell Biol.* **6**, 731–740 (2004).
32. B. Dai, W. Wan, P. Zhang, Y. Zhang, C. Pan, G. Meng, X. Xiao, Z. Wu, W. Jia, J. Zhang, L. Zhang, SET and MYND domain-containing protein 3 is overexpressed in human glioma and contributes to tumorigenicity. *Oncol. Rep.* **34**, 2722–2730 (2015).
33. R. Hamamoto, F. P. Silva, M. Tsuge, T. Nishidate, T. Katagiri, Y. Nakamura, Y. Furukawa, Enhanced SMYD3 expression is essential for the growth of breast cancer cells. *Cancer Sci.* **97**, 113–118 (2006).
34. C. Liu, C. Wang, K. Wang, L. Liu, Q. Shen, K. Yan, X. Sun, J. Chen, J. Liu, H. Ren, H. Liu, Z. Xu, S. Hu, D. Xu, Y. Fan, SMYD3 as an oncogenic driver in prostate cancer by stimulation of androgen receptor transcription. *J. Natl. Cancer Inst.* **105**, 1719–1728 (2013).

35. F. Q. Vieira, P. Costa-Pinheiro, D. Almeida-Rios, I. Graca, S. Monteiro-Reis, S. Simões-Sousa, I. Carneiro, E. J. Sousa, M. I. Godinho, F. Baltazar, R. Henrique, C. Jeronimo, SMYD3 contributes to a more aggressive phenotype of prostate cancer and targets Cyclin D2 through H4K20me3. *Oncotarget* **6**, 13644–13657 (2015).
36. B. K. Yoo, P. K. Santhekadur, R. Gredler, D. Chen, L. Emdad, S. Bhutia, L. Pannell, P. B. Fisher, D. Sarkar, Increased RNA-induced silencing complex (RISC) activity contributes to hepatocellular carcinoma. *Hepatology* **53**, 1538–1548 (2011).
37. M. A. Blanco, M. Aleckovic, Y. Hua, T. Li, Y. Wei, Z. Xu, I. M. Cristea, Y. Kang, Identification of staphylococcal nuclease domain-containing 1 (SND1) as a Metadherin-interacting protein with metastasis-promoting functions. *J. Biol. Chem.* **286**, 19982–19992 (2011).
38. H. Kuruma, Y. Kamata, H. Takahashi, K. Igarashi, T. Kimura, K. Miki, J. Miki, H. Sasaki, N. Hayashi, S. Egawa, Staphylococcal nuclease domain-containing protein 1 as a potential tissue marker for prostate cancer. *Am. J. Pathol.* **174**, 2044–2050 (2009).
39. N. Wang, X. Du, L. Zang, N. Song, T. Yang, R. Dong, T. Wu, X. He, J. Lu, Prognostic impact of Metadherin–SND1 interaction in colon cancer. *Mol. Biol. Rep.* **39**, 10497–10504 (2012).
40. L. Emdad, A. Janjic, M. A. Alzubi, B. Hu, P. K. Santhekadur, M. E. Menezes, X.-N. Shen, S. K. Das, D. Sarkar, P. B. Fisher, Suppression of miR-184 in malignant gliomas upregulates SND1 and promotes tumor aggressiveness. *Neuro Oncol.* **17**, 419–429 (2015).
41. J. J. Raizer, W.-J. Hwu, K. S. Panageas, A. Wilton, D. E. Baldwin, E. Bailey, C. von Althann, L. A. Lamb, G. Alvarado, M. H. Bilsky, P. H. Gutin, Brain and leptomeningeal metastases from cutaneous melanoma: Survival outcomes based on clinical features. *Neuro Oncol.* **10**, 199–207 (2008).
42. J. Mazar, K. DeYoung, D. Khaitan, E. Meister, A. Almodovar, J. Goydos, A. Ray, R. J. Perera, The regulation of miRNA-211 expression and its role in melanoma cell invasiveness. *PLOS ONE* **5**, e13779 (2011).
43. Y. Zhang, T. Liu, C. A. Meyer, J. Eeckhoute, D. S. Johnson, B. E. Bernstein, C. Nusbaum, R. M. Myers, M. Brown, W. Li, X. S. Liu, Model-based analysis of ChIP-Seq (MACS). *Genome Biol.* **9**, R137 (2008).
44. M. Martin, Cutadapt removes adapter sequences from high-throughput sequencing reads. *EMBnet.journal* **17**, 10–12 (2011).
45. B. Langmead, C. Trapnell, M. Pop, S. L. Salzberg, Ultrafast and memory-efficient alignment of short DNA sequences to the human genome. *Genome Biol.* **10**, R25 (2009).
46. S. Aviran, C. Trapnell, J. B. Lucks, S. A. Mortimer, S. Luo, G. P. Schroth, J. A. Doudna, A. P. Arkin, L. Pachter, Modeling and automation of sequencing-based characterization of RNA structure. *Proc. Natl. Acad. Sci. U.S.A.* **108**, 11069–11074 (2011).
47. K. Darty, A. Denise, Y. Ponty, VARNA: Interactive drawing and editing of the RNA secondary structure. *Bioinformatics* **25**, 1974–1975 (2009).
48. M. Batish, P. van den Bogaard, F. R. Kramer, S. Tyagi, Neuronal mRNAs travel singly into dendrites. *Proc. Natl. Acad. Sci. U.S.A.* **109**, 4645–4650 (2012).
49. F. B. Markey, W. Ruezinsky, S. Tyagi, M. Batish, Fusion FISH imaging: Single-molecule detection of gene fusion transcripts in situ. *PLOS ONE* **9**, e93488 (2014).
50. M. N. Cabili, M. C. Dunagin, P. D. McClanahan, A. Biaesch, O. Padovan-Merhar, A. Regev, J. L. Rinn, A. Raj, Localization and abundance analysis of human lncRNAs at single-cell and single-molecule resolution. *Genome Biol.* **16**, 20 (2015).
51. A. Lin, R. T. Wang, S. Ahn, C. C. Park, D. J. Smith, A genome-wide map of human genetic interactions inferred from radiation hybrid genotypes. *Genome Res.* **20**, 1122–1132 (2010).
52. W. Ritchie, S. Flamant, J. E. J. Rasko, Predicting microRNA targets and functions: Traps for the unwary. *Nat. Methods* **6**, 397–398 (2009).

Acknowledgments: We thank Sanford Burnham Prebys Medical Discovery Institute Analytical Genomics Core Facility for deep sequencing, Bioinformatics Core for data analysis support, Histology Core, and Microscope Facility for immunohistochemistry studies, and D. McFadden (Sanford Burnham Prebys Medical Discovery Institute) for formatting the manuscript. **Funding:** This work was supported by NIH grants CA165184 and NCI 5P30CA030199 and Florida Department of Health, Bankhead-Coley Cancer Research Program 5BC08 to R.J.P. and NIH grant DP5 OD012160 to M.B. A.R. is funded by the U.S. Department of Defense (CDMRP #LC150653). **Author contributions:** B.L., A.R., and R.J.P. incepted the idea, planned the experiment, analyzed data, and wrote the manuscript. A.S. provided support in mouse xenograft studies. E.H., X.C., J.-L.L., S.J.L., T.S., and S.Z. were involved in dChIRP data analysis, SHAPE-seq data analysis, and building of SPRIGHTLY-interacting networks and pathways. J.M. and S.S.G. provided support in generating RNA-seq and SHAPE-seq data. F.B.M. conducted the RNA-FISH experiment. M.B. conducted the RNA-FISH experiment and data analysis. **Competing interests:** The authors declare that they have no competing interests. **Data and materials availability:** All data needed to evaluate the conclusions in the paper are present in the paper and/or the Supplementary Materials. Additional data related to this paper may be requested from the authors. We do not have any materials obtained through a material transfer agreement. Cell lines and mice were purchased. Data are archived (GSE95597).

Submitted 14 October 2016
Accepted 3 March 2017
Published 3 May 2017
10.1126/sciadv.1602505

Citation: B. Lee, A. Sahoo, J. Marchica, E. Holzhauser, X. Chen, J.-L. Li, T. Seki, S. S. Govindarajan, F. B. Markey, M. Batish, S. J. Lokhande, S. Zhang, A. Ray, R. J. Perera, The long noncoding RNA *SPRIGHTLY* acts as an intranuclear organizing hub for pre-mRNA molecules. *Sci. Adv.* **3**, e1602505 (2017).

ScienceAdvances
AAAS

The long noncoding RNA *SPRIGHTLY* acts as an intranuclear organizing hub for pre-mRNA molecules

Bongyong Lee, Anupama Sahoo, John Marchica, Erwin Holzhauser, Xiaoli Chen, Jian-Liang Li, Tatsuya Seki, Subramaniam Shyamala Govindarajan, Fatu Badiane Markey, Mona Batish, Sonali J. Lokhande, Shaojie Zhang, Animesh Ray and Ranjan J. Perera (May 3, 2017)

Sci Adv 2017, 3:.
doi: 10.1126/sciadv.1602505